Scientia Iranica B (2021) 28(3), 1329–1341

Sharif University of Technology
Scientia Iranica
Transactions B: Mechanical Engineering
http://scientiairanica.sharif.edu

Research Note

Cattaneo-Christov heat and mass flux models on time-dependent swirling flow through oscillatory rotating disk

Z. Abbas[a], A. Rauf[a,b,*], S.A. Shehzad[b], and M. Alghamdi[c]

a. *Department of Mathematics, The Islamia University of Bahawalpur, Bahawalpur, 63100, Pakistan.*
b. *Department of Mathematics, COMSATS University Islamabad, Sahiwal Campus, 57000, Pakistan.*
c. *Department of Mathematics, Faculty of Science, King Khalid University, Abha 61413, Saudi Arabia.*

Received 30 March 2019; received in revised form 16 December 2019; accepted 13 July 2020

KEYWORDS
Unsteady flow;
Porous medium;
Magnetohydrodynamics;
Cattaneo-Christov theory;
Numerical solution.

Abstract. In this paper, the time invariant impressions of Cattaneo-Christov heat and mass flux theories were implemented to overcome the initial instant disturbances throughout whole medium. The motion of three-dimensional, incompressible, magnetized viscous fluid flow was induced by the oscillatory disk. Porous media was used to saturate the rotating disk. Similarity transformations were accomplished to normalize the flow problem. Successive Over Relaxation (SOR) technique was implemented to discuss the new findings of normalized non-linear resulting system. It is perceived that increase in porosity parameter results in decrease of oscillatory velocity profiles. The characterization of porous media is useful in geothermal and petroleum reservoirs. Time varying oscillatory curves for concentration and temperature decay for varying concentration and thermal relaxation time parameters, respectively. Moreover, the interesting nature of phase-log shift is also observed in temperature and concentration profiles. Three-dimensional flow features are also labeled for velocity, temperature and concentration fields.

1. Introduction

The combined heat-mass transportation emerges frequently in widespread manufacturing and industrial wise applications like nuclear processes, nuclear reactor, cooling processes, hot wiring, distillation columns, power generation, marine engineering, solar technology, transpiration processes, packed bed processes, production of glass-fiber, furnace design and energy production. Heat conduction Fourier's law is the most famous model in the field of continuum mechanics. Differential equation of parabolic type for temperature is obtained by Fourier's law and has major short comings of having instant initial disturbances throughout whole medium. Such unrealistic feature was termed as paradox of heat conduction. These various techniques have been implemented over time, however all of them have not been utilized successfully [1].

Maxwell-Cattaneo law [2] is one of those techniques in which time partial derivative is added in constitutive equation by Cattaneo. The law overcome the shortcoming of Fourier's law by acquiring damped hyperbolic equation and describe relationship among temperature flourished and heat flux. Khan et al. [3] communicated the series solutions by implementing Homotopy Analysis Method (HAM) of the problem of three-dimensional Burgers fluid flow through stretch-

*. *Corresponding author. Tel.: +92332-7760605*
E-mail address: raufamar@cuisahiwal.edu.pk (A. Rauf)

doi: 10.24200/sci.2020.53248.3139

ing surface with characterization of Cattaneo-Christov model of heat and mass flux theories. Liu et al. [4] obtained numerical solutions to feature the heat conduction influence by characterizing Cattaneo-Christov theory using space fractional derivative. Upadhay et al. [5] computed numerical solutions of dusty Eyring-Powell nanofluid flow over stretching sheet subject to Cattaneo-Christov model. The implementation of HAM is utilized to study the salient features of Cattaneo-Christov heat-mass flux theories on squeezing fluid flow by Farooq et al. [6]. Shehzad et al. [7] computed analytical simulations to visualize the characteristics to Cattaneo-Christov heat-mass flux theories on flow of Maxwell liquid through moving surface. Rauf et al. [8] analyzed the flow features of Powell-Eyring liquid through stretching surface using Cattaneo-Christov heat-mass diffusion in numerical sense via (SOR) technique. Aqsa et al. [9] investigated the Burger's fluid flow by considering the model of Cattaneo-Christov. Khan et al. [10] elaborated the results of second grade viscoelastic fluid model by using the non-Fourier's formula of heat diffusion.

Rotating flows have fascinating phenomenon because of the richness involved in scientific and engineering applications. Understanding such phenomenon provides modeling capabilities to design turbomachines and various other products for power plants, turbo machinery, oil industry and medical engineering such as jet engines, vacuum cleaners pumps and swirl flow through diffuser. Especially fluid flow subjected to the oscillatory motion of rotating surfaces has innumerous practical applications worldwide. The analysis of such type incorporates the thermal stability analysis of chemical reactors, thermal radiators, condensers, separation systems, centrifuges, radiators, centrifugal pumps, heat exchangers, jet engines and designing process of the thermal subsystems as implication in boilers. Chawla et al. [11] examined incompressible flow of viscous fluid subjected to porous rotating disk. Mahmood et al. [12] obtained numerical solutions for unsteady viscous fluid flow through rotating disc, lubricated by thin coating of power-law fluid. Yin et al. [13] executed analytical technique to discuss heat transfer attributes of nanofluid flow across rotating disk. Mustafa [14] accomplished numerical technique to analyze the distinctions of nanofluid due to rotating disk. Turkyilmazoglu [15] investigated heat transfer phenomenon of viscous fluid flow near vertically moving and rotating disk. Lok et al. [16] established numerical solutions of stagnation-point flow through permeable rotating disk of stretching/shrinking type. Hayat et al. [17] obtained series solutions by adopting HAM to study the entropy generation of Sisko fluid flow by rotating disk. Gholinia et al. [18] attained numerical solutions for flow problem of Eyring-Powell fluid via rotating disk.

The topic of porous media with applications in industry and engineering is an active area of research. The pioneer work in fluid transport area and heat transport through porous media started from the last century. The applications of such fascinating area were found in thermal-insulation engineering, chemical waste spreading, geothermal reservoirs, petroleum reservoirs, grain storage, catalytic reactors, coal combustors and microsphere insulation of packed cryogenic [19–25]. On basis of such specific applications of porous media, the flow may be external or internal through porous medium. In this regard, most of the research work was done by implementing Darcy law [26]. The model based on the creeping flow assumption is subject to infinitely enlarged uniform medium such that average volume velocity and pressure gradient keeps direct relationship [27]. Khan et al. [28] solved the problem of second grade fluid flow through oscillatory moving surface submerged into porous medium. Ali et al. [29] performed simulations using HAM to discuss the flow characteristics of couple stress fluid via oscillatory sheet subjected to porous medium. Ali et al. [30] discussed the flow problem of viscoelastic fluid through oscillatory moving sheet via porous medium. Hasnain and Abbas [31] examined flow of two immiscible liquids through inclined annulus of concentric cylinders in porous medium. Sheikholeslami and Shehzad [32] performed numerical simulation using Control Volume Finite Element Method (CVFEM) to analyze heat transfer features of nanoparticles in an enclosure merged in porous medium. Sheikholeslami et al. [33] discussed the nanofluid flow behavior through oscillatory vertical plate, taking place in porous medium.

The main goal of our study is to study the numerical findings of incompressible, three-dimensional MHD flow of viscous fluid. The motion of fluid is generated due to oscillatory rotating disk saturated by the porous space. One of premier imperfections of Fourier's theory is that temperature field is parabolic in nature due to which early disturbance is detected all over the medium. Such behavior contradicts with causality principle. To rectify such unrealistic attribute, Christov [2] include time derivative term in constitutive expression between temperature and heat flux which extends the heat equation into damped hyperbolic one and solves the major short comings in Fourier's model. Therefore the utilization of Cattaneo-Christov heat and mass flux theories is made for the present flow problem. The magnetized flow problems of viscous material through rotation of oscillatory disk under double diffusive Cattaneo-Christov theory have not still been studied in literature. The present work is the extension of [34] with addition of Cattaneo-Christov theories of double diffusion. Mathematical model is developed in Section 2. Section 3 mentions the numerical solutions. Discussions of results are elaborated in Section 4. Conclusions are discussed in Section 5.

2. Mathematical modeling

A three-dimensional, unsteady, incompressible flow of hydromagnetic viscous fluid is assessed. Constant rotation and periodic oscillation of the disk is generated by the fluid motion and the disk is equipped in porous space. Angular speed of disk is γ and amplitude of oscillation is denoted by ε. The disk is located in $z = 0$ plane. Most appropriate choice, here, is to choose system of cylindrical co-ordinates such that the components of velocity (u, v, w) are considered along (r, θ, z) direction. Flow is assumed to be axi-symmetric, therefore derivatives are neglected along tangential component. Electric field is ignored because of low Reynolds number. Uniform potency magnetic field is employed in the axial direction. Heat and mass transfer features are inspected by utilizing modified form of Fick and Fourier's laws namely Cattaneo-Christov mass and heat flux theories.

Temperature and concentration at wall are denoted by T_w and C_w whereas ambient temperature and concentration are determined by T_∞ and C_∞. Figure 1 explains the geometrical configuration.

Considering the above assumptions, the mathematical model is [2,35–37]:

$$\frac{\partial u}{\partial r} + \frac{u}{r} + \frac{\partial w}{\partial z} = 0, \tag{1}$$

$$\frac{\partial u}{\partial t} + u\frac{\partial u}{\partial r} - \frac{\nu^2}{r} + w\frac{\partial u}{\partial z} = -\frac{1}{\rho}\frac{\partial p}{\partial r} + \nu\left(\frac{\partial^2 u}{\partial r^2} + \frac{\partial}{\partial r}\left(\frac{u}{r}\right) + \frac{\partial^2 u}{\partial z^2}\right) - \frac{\sigma_e \beta_0^2 u}{\rho} - \frac{\mu\phi_1}{\rho k_1}u, \tag{2}$$

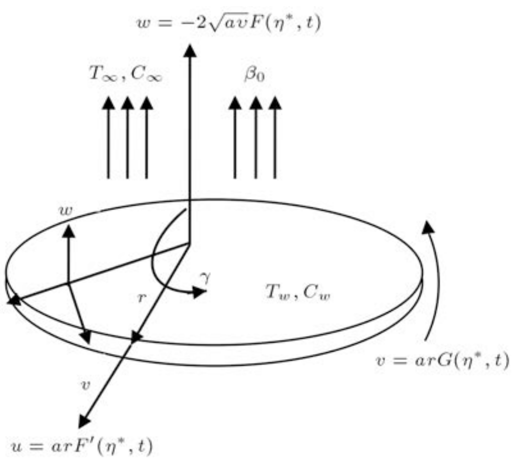

Figure 1. Geometry of the problem.

$$\frac{\partial v}{\partial t} + u\frac{\partial \nu}{\partial r} + \frac{u\nu}{r} + w\frac{\partial \nu}{\partial z} = \upsilon\left(\frac{\partial^2 \nu}{\partial r^2} + \frac{\partial}{\partial r}\left(\frac{\nu}{r}\right) + \frac{\partial^2 \nu}{\partial z^2}\right) - \frac{\sigma_e \beta_0^2 \nu}{\rho} - \frac{\mu\phi_1}{\rho k_1}\nu, \tag{3}$$

$$\frac{\partial w}{\partial t} + u\frac{\partial w}{\partial r} + w\frac{\partial w}{\partial z} = -\frac{1}{\rho}\frac{\partial p}{\partial z} + \upsilon\left(\frac{\partial^2 w}{\partial r^2} + \frac{1}{r}\frac{\partial w}{\partial r} + \frac{\partial^2 w}{\partial z^2}\right) - \frac{\mu\phi_1}{\rho k_1}w, \tag{4}$$

$$\begin{aligned}\frac{\partial T}{\partial t} + u\frac{\partial T}{\partial r} + w\frac{\partial T}{\partial z} &= \alpha\left(\frac{\partial^2 T}{\partial r^2} + \frac{1}{r}\frac{\partial T}{\partial r} + \frac{\partial^2 T}{\partial z^2}\right) \\ &- \tau_0\Bigg(\frac{\partial^2 T}{\partial t^2} + u\frac{\partial u}{\partial r}\frac{\partial T}{\partial r} + w\frac{\partial w}{\partial z}\frac{\partial T}{\partial z} + u\frac{\partial w}{\partial r}\frac{\partial T}{\partial z} \\ &+ w\frac{\partial u}{\partial z}\frac{\partial T}{\partial r} + 2uw\frac{\partial^2 T}{\partial r\partial z} + u^2\frac{\partial^2 T}{\partial r^2} + w^2\frac{\partial^2 T}{\partial z^2} \\ &+ \frac{\partial u}{\partial t}\frac{\partial T}{\partial r} + 2u\frac{\partial^2 T}{\partial r\partial r} + \frac{\partial w}{\partial t}\frac{\partial T}{\partial z} + 2w\frac{\partial^2 T}{\partial z\partial t}\Bigg),\end{aligned} \tag{5}$$

$$\begin{aligned}\frac{\partial C}{\partial t} + u\frac{\partial C}{\partial r} + w\frac{\partial C}{\partial z} &= D_B\left(\frac{\partial^2 C}{\partial r^2} + \frac{1}{r}\frac{\partial C}{\partial r} + \frac{\partial^2 C}{\partial z^2}\right) \\ &- \tau_1\Bigg(\frac{\partial^2 C}{\partial t^2} + u\frac{\partial u}{\partial r}\frac{\partial C}{\partial r} + w\frac{\partial w}{\partial z}\frac{\partial C}{\partial z} + u\frac{\partial w}{\partial r}\frac{\partial C}{\partial z} \\ &+ w\frac{\partial u}{\partial z}\frac{\partial C}{\partial r} + 2uw\frac{\partial^2 C}{\partial r\partial z} + u^2\frac{\partial^2 C}{\partial r^2} + w^2\frac{\partial^2 C}{\partial z^2} \\ &+ \frac{\partial u}{\partial t}\frac{\partial C}{\partial r} + 2u\frac{\partial^2 C}{\partial r\partial r} + \frac{\partial w}{\partial t}\frac{\partial C}{\partial z} + 2w\frac{\partial^2 C}{\partial z\partial t}\Bigg).\end{aligned} \tag{6}$$

The associated boundary conditions for $(t > 0)$ are [37]:

at $z = 0$:

$$u(r, z; t) = ar(1 + \varepsilon \sin \omega t), \qquad \nu(r, z; t) = \gamma r,$$

$$w(r, z; t) = 0, \qquad T(r, z; t) = T_w, \qquad C(r, z; t) = C_w$$

when $z \to \infty$:

$$u(r, z; t) \to 0, \qquad \nu(r, z; t) \to 0, \qquad w(r, z; t) \to 0,$$

$$T(r, z; t) \to T_\infty, \qquad C(r, z; t) \to C_\infty, \tag{7}$$

and initial conditions are [37]:

$$u = 0, \quad \nu = 0, \quad w = 0 \quad \text{at} \quad t = 0 \quad \text{for all } r \text{ and } z. \tag{8}$$

Here υ, ρ, and μ represent the kinematic viscosity, density and dynamic viscosity, β_0 the magnetic flux density, σ_e the electrical conductivity, ϕ_1 and k_1 the porosity and permeability of porous medium, $\alpha = \frac{k}{\rho c_p}$

co-efficient of heat diffusion, D_B Brownian diffusion coefficient, τ_0 heat flux relaxation time, ω the angular frequency, and τ_1 the concentration relaxation time. The self-similar variables are expressed as [37]:

$$u = arF'(\eta^*, t^*), \qquad \nu = arG(\eta^*, t^*),$$

$$w = -2\sqrt{av}F(\eta^*, t^*), \qquad p = \rho av P(\eta^*, t^*)$$

$$\theta(\eta^*, t^*) = \frac{T - T_\infty}{T_w - T_\infty}, \qquad \phi(\eta^*, t^*) = \frac{C - C_\infty}{C_w - C_\infty},$$

$$\eta^* = \sqrt{\frac{a}{v}}z, \qquad t^* = \omega t. \tag{9}$$

Self-similar transformations reduce Eqs. (1)–(7) into the following:

$$F''' - (F')^2 + 2FF'' - StF'_t + G^2 - \left(M^2 + P\right) F' = 0, \tag{10}$$

$$G'' - 2F'G + 2FG'_t - \left(M^2 + P\right) G - StG = 0, \tag{11}$$

$$\theta'' + \Pr\left(2F\theta' - St\theta_t - \lambda_1\left(4FF'\theta' + St^2\theta_{tt} + 4F^2\theta'' - 2StF_t\theta' - 4StF\theta'_t\right)\right) = 0, \tag{12}$$

$$\phi'' + \mathrm{Sc}\left(2F\phi' - St\phi_t - \lambda_2\left(4FF'\phi' + St^2\phi_{tt} + 4F^2\phi'' - 2StF_t\phi' - 4StF\phi'_t\right)\right) = 0, \tag{13}$$

and boundary conditions transform to the following:

$$F(0,t) = 0, \qquad F'(0,t) = 1 + \varepsilon \sin t, \qquad G(0,t) = \Omega,$$

$$\theta(0,t) = 1, \qquad \phi(0,t) = 1, \qquad P(0,t) = 0,$$

$$F'(\infty,t) \to 0, \qquad G(\infty,t) \to 0, \qquad \theta(\infty,t) \to 0,$$

$$\phi(\infty,t) \to 0, \tag{14}$$

where prime ($'$) denotes the differentiation with respect to the dimensionless variable z; the subscript t represents the differentiation with respect to the dimensionless time t; $St = \frac{\omega}{a}$ the unsteady parameter; $M = \sqrt{\frac{\sigma_e \beta_0^2}{a\rho}}$ the magnetic parameter; $P = \frac{\mu\phi_1}{a\rho k_1}$ the porosity parameter; $\Pr = \frac{v}{\alpha}$ the Prandtl number; $\Omega = \frac{\gamma}{a}$ the swirl parameter; $\lambda_1 = a\tau_0$ the thermal relaxation time parameter; $\lambda_2 = a\tau_1$ the concentration relaxation time parameter; and $\mathrm{Sc} = \frac{v}{D_B}$ stands for Schmidt number.

Shear stresses at the disk surface are defined as:

$$\tau_{zr} = \mu \frac{\partial u}{\partial z}\bigg|_{z=0} = \mu a \mathrm{Re}_x^{\frac{1}{2}} F''(0,t),$$

$$\tau_{z\theta} = \mu \frac{\partial \nu}{\partial z}\bigg|_{z=0} = \mu a \mathrm{Re}_x^{\frac{1}{2}} G'(0,t). \tag{15}$$

Here $\mathrm{Re}_x = \frac{ar^2}{v}$ stands for Local Reynolds number.

3. Numerical solution

The resulting system of equations is of the second order in G, θ, and ϕ, and third order in F. Eq. (10) is converted into second order using technique of order reduction as follows:

$$F' = X, \tag{16}$$

$$X'' + 2FX' - X^2 + G^2 - StX_t - (M^2 + P)X = 0, \tag{17}$$

$$G'' - 2XG + 2FG' - StG_t - (M^2 + P)G = 0, \tag{18}$$

$$\theta'' + \Pr(2F\theta' - St\theta_t - \lambda_1(St^2\theta_{tt} + 4FX\theta' + 4F^2\theta'' - 2F_t\theta' St - 4F\theta'_t St)) = 0, \tag{19}$$

$$\phi'' + \mathrm{Sc}(2F\phi' - St\phi_t - \lambda_2(St^2\phi_{tt} + 4FX\phi' + 4F^2\phi'' - 2F_t\phi' St - 4F\phi'_t St)) = 0. \tag{20}$$

Boundary conditions (Eq. (14)) in terms of Eq. (16) become:

$$F(0,t) = 0, \qquad X(0,t) = 1 + \varepsilon \sin t, \qquad G(0,t) = \Omega,$$

$$\theta(0,t) = 1, \qquad \phi(0,t) = 1, \qquad P(0,t) = 0,$$

$$X(\infty,t) \to 0, \qquad G(\infty,t) \to 0, \qquad \theta(\infty,t) \to 0,$$

$$\phi(\infty,t) \to 0. \tag{21}$$

Domain truncation technique is implemented in order to obtain finite domain $[0, N]$ from semi-infinite domain $[0, \infty)$. Boundary conditions which are utilized at infinity are mentioned at end point N of domain. The uniformly distributed $R + 1$ points that are discretize with variable η subject to the step-size is chosen to be $\delta\eta = \frac{N}{R}$. The resulting system is then solved through numerical way by implementing finite differences discretization scheme. The backward difference formulas of first and second orders are approximated with respect to time as follows:

$$\frac{\partial X}{\partial t} \approx \frac{X_{i,j} - X_{i,j-1}}{\delta t}, \qquad \frac{\partial G}{\partial t} \approx \frac{G_{i,j} - G_{i,j-1}}{\delta t},$$

$$\frac{\partial \theta}{\partial t} \approx \frac{\theta_{i,j} - \theta_{i,j-1}}{\delta t}, \qquad \frac{\partial^2 \theta}{\partial t^2} \approx \frac{\theta_{i,j} - 2\theta_{i,j-1} + \theta_{i,j-2}}{\delta t^2},$$

$$\frac{\partial \phi}{\partial t} \approx \frac{\phi_{i,j} - \phi_{i,j-1}}{\delta t}, \qquad \frac{\partial^2 \phi}{\partial t^2} \approx \frac{\phi_{i,j} - 2\phi_{i,j-1} + \phi_{i,j-2}}{\delta t^2}. \tag{22}$$

Central difference approximations of first and second orders are approximated with respect to η as:

$$\frac{\partial Y}{\partial \eta} \approx \frac{Y_{i+1,j} - Y_{i-1,j}}{2\delta\eta}, \qquad \frac{\partial G}{\partial \eta} \approx \frac{G_{i+1,j} - G_{i-1,j}}{2\delta\eta},$$

$$\frac{\partial \theta}{\partial \eta} \approx \frac{\theta_{i+1,j} - \theta_{i-1,j}}{2\delta\eta}, \qquad \frac{\partial \phi}{\partial \eta} \approx \frac{\phi_{i+1,j} - \phi_{i-1,j}}{2\delta\eta},$$

$$\frac{\partial^2 Y}{\partial \eta^2} \approx \frac{Y_{i+1,j} - 2Y_{i,j} + Y_{i-1,j}}{\delta\eta^2},$$

$$\frac{\partial^2 G}{\partial \eta^2} \approx \frac{G_{i+1,j} - 2G_{i,j} + G_{i-1,j}}{\delta\eta^2},$$

$$\frac{\partial^2 \theta}{\partial \eta^2} \approx \frac{\theta_{i+1,j} - 2\theta_{i,j} + \theta_{i-1,j}}{\delta\eta^2},$$

$$\frac{\partial^2 \phi}{\partial \eta^2} \approx \frac{\phi_{i+1,j} - 2\phi_{i,j} + \phi_{i-1,j}}{\delta\eta^2}. \tag{23}$$

Here i and j are taken as spatial and time levels, respectively.

Eqs. (16)–(21) in view of Eqs. (22) and (23) are written as:

$$\left(-X_{i,j} - \frac{2}{\delta\eta^2} - \frac{St}{\delta t} - M^2 - P\right) Y_{i,j} + \left(\frac{1}{\delta\eta^2} + \frac{F_{i,j}}{\delta\eta}\right) X_{i+1,j} + \left(\frac{1}{\delta\eta^2} - \frac{F_{i,j}}{\delta\eta}\right) X_{i-1,j} + G_{i,j}^2 + \frac{St}{\delta t} X_{i,j-1} = 0, \tag{24}$$

$$\left(-\frac{2}{\delta\eta^2} - X_{i,j} - \frac{St}{\delta t} - M^2 - P\right) G_{i,j} + \left(\frac{1}{\delta\eta^2} + \frac{F_{i,j}}{\delta\eta}\right) G_{i+1,j} + \left(\frac{1}{\delta\eta^2} - \frac{F_{i,j}}{\delta\eta}\right) G_{i-1,j} + \frac{St}{\delta t} G_{i,j-1} = 0, \tag{25}$$

$$\left(\frac{1}{\delta\eta^2} + \frac{\mathrm{Pr}F_{i,j}}{\delta\eta} - \frac{2\mathrm{Pr}\lambda_1 F_{i,j}Q_{i,j}}{\delta\eta} - \frac{4\mathrm{Pr}\lambda_1 F_{i,j}^2}{\delta\eta^2} + \frac{St(F_{ij} - F_{i,j-1})}{dt\delta\eta}\right)\theta_{i+1,j} + \left(\frac{St\mathrm{Pr}}{\delta t} + \frac{2\mathrm{Pr}\lambda_1 St^2}{dt^2}\right)\theta_{i,j-1} - \left(\frac{\mathrm{Pr}\,\lambda_1 St^2}{dt^2}\right)\theta_{i,j-2} + \left(\frac{1}{\delta\eta^2} - \frac{\mathrm{Pr}F_{i,j}}{\delta\eta} - \frac{2\mathrm{Pr}\lambda_1 F_{i,j}Q_{i,j}}{\delta\eta} - \frac{4\mathrm{Pr}\lambda_1 F_{i,j}^2}{\delta\eta^2} - \frac{St(F_{i,j} - F_{i,j-1})}{dt\delta\eta}\right)\theta_{i-1,j} - \left(\frac{2}{\delta\eta^2} + \frac{St\mathrm{Pr}}{\delta t} + \frac{\mathrm{Pr}\lambda_1 St^2}{dt^2} - \frac{8\mathrm{Pr}\lambda_1 F_{i,j}^2}{\delta\eta^2}\right)\theta_{i,j} + \frac{2\mathrm{Pr}\lambda_1 St(\theta_{i+1,j-1} - \theta_{i-1,j-1})}{dt\delta\eta} = 0, \tag{26}$$

$$\left(\frac{1}{\delta\eta^2} + \frac{\mathrm{Sc}F_{i,j}}{\delta\eta} - \frac{2\mathrm{Sc}\lambda_2 F_{i,j}Q_{i,j}}{\delta\eta} - \frac{4\mathrm{Sc}\lambda_2 F_{i,j}^2}{\delta\eta^2} + \frac{St(F_{ij} - F_{i,j-1})}{dt\delta\eta}\right)\phi_{i+1,j} + \left(\frac{St\mathrm{Sc}}{\delta t} + \frac{2\mathrm{Sc}\lambda_2 St^2}{dt^2}\right)\phi_{i,j-1} - \left(\frac{\mathrm{Sc}\lambda_2 St^2}{dt^2}\right)\phi_{i,j-2} + \left(\frac{1}{\delta\eta^2} - \frac{\mathrm{Sc}F_{i,j}}{\delta\eta} - \frac{2\mathrm{Sc}\lambda_2 F_{i,j}Q_{i,j}}{\delta\eta} - \frac{4\mathrm{Sc}\lambda_2 F_{i,j}^2}{\delta\eta^2} - \frac{St(F_{i,j} - F_{i,j-1})}{dt\delta\eta}\right)\phi_{i-1,j} - \left(\frac{2}{\delta\eta^2} + \frac{St\mathrm{Sc}}{\delta t} + \frac{\mathrm{Sc}\lambda_2 St^2}{dt^2} - \frac{8\mathrm{Sc}\lambda_2 F_{i,j}^2}{\delta\eta^2}\right)\phi_{i,j} + \frac{2\mathrm{Sc}\lambda_2 St(\phi_{i+1,j-1}, \phi_{i-1,j-1})}{dt\delta\eta} = 0. \tag{27}$$

Here boundary conditions [21] take the following form:

$$F_{0,j} = 0, \qquad Y_{0,j} = 1 + \varepsilon \sin t_k, \qquad G_{0,j} = \Omega,$$

$$\theta_{0,j} = 1, \qquad \phi_{0,j} = 1,$$

$$Y_{N,j} = G_{N,j} = \theta_{N,j} = \phi_{N,j} = 0. \tag{28}$$

SOR is enforced for an iterative process to obtain numerical solution. Further equation (Eq. (16)) is integrated using Milne and Adam Moulton methods [38]. In our numerical method, the optima value of successive over relaxation parameter is taken $\omega = 1.95$. A spectral radius convergence criterion is expressed by [39]:

$$\rho(G_\omega) = \begin{cases} \frac{1}{4}\left(\omega\rho + \sqrt{(\omega\rho)^2 - 4(\omega - 1)}\right)^2 \\ \quad \text{for} \quad 0 < \omega \le \omega_{opt} \\ \omega - 1 \\ \quad \text{for} \quad \omega_{opt} \le \omega < 2 \end{cases} \tag{29}$$

Here the optimal relaxation parameter is calculated by:

$$\omega_{opt} = 1 + \left(\frac{\rho(G_{\mathrm{Jac}})}{1 + \sqrt{1 - (\rho(G_{\mathrm{Jac}}))^2}}\right)^2, \tag{30}$$

where $\rho(G_{\mathrm{Jac}})$ denotes spectral radius of Jacobi method. In current process of execution, we used time scales $t_k = k\delta t$, $k = 0, 1, 2, \cdots$.

4. Discussion of the results

Numerical analysis is implemented to study the unsteady, hydromagnetic flow problem of viscous fluid

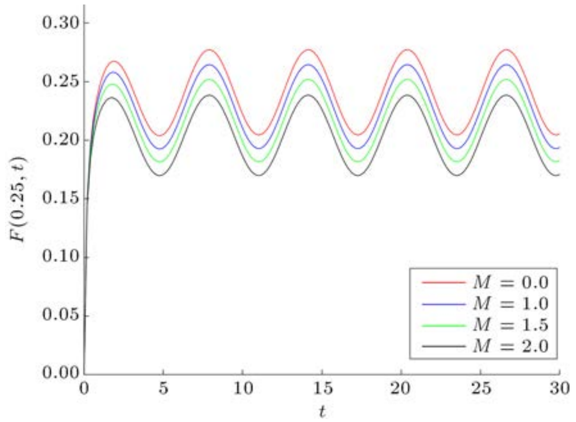

Figure 2. Out-turns of M on F at $\eta = 0.25$.

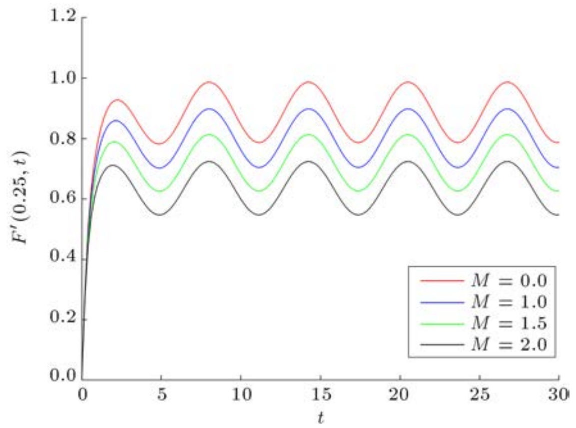

Figure 3. Out-turns of M on F' at $\eta = 0.25$.

by implementing modified forms of heat and mass flux theories subjected to oscillatory disk. The disk takes its place in porous space. Analysis is carried out to discuss the results of dimensionless quantities through graphical representations and in tabular view forms. The physical parameters, which are under consideration, are magnetic parameter, porosity parameter, swirl parameter, constant amplitude, Prandtl number, Schmidt number and thermal and concentration relaxation time parameters. The graphs of various magnetic parameter values $M = 0, 1, 1.5, 2$ on $F'(0.25, t)$ and $F(0.25, t)$ are demonstrated in Figures 2 and 3, respectively. The fluid flow becomes hydrodynamic under the situation when $M = 0$. By introducing the magnetic field, a force termed Lorentz force evolves in flow field. Such force is responsible for producing resistance and hence reducing velocity graphs. Furthermore, in Figure 2, the axial velocity $F(0.25, t)$ curves are more close to each other and domain of oscillation is small in comparison to radial velocity $F'(0.25, t)$ profiles in Figure 3. The demonstration of porosity parameter on both axial and radial velocities is pictured in Figures 4 and 5. Similar observation is perceived in graphical results for varying porosity parameter as in the scenario of magnetic parameter. The porosity parameter has also

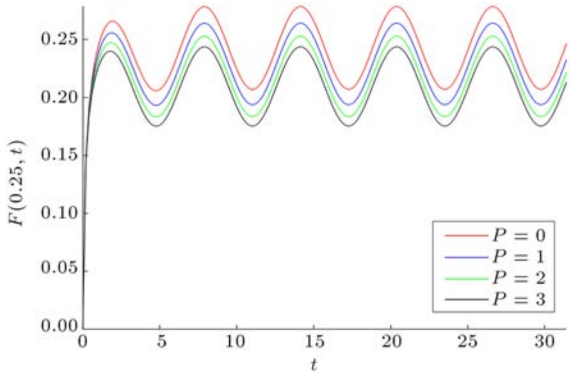

Figure 4. Out-turns of P on F at $\eta = 0.25$.

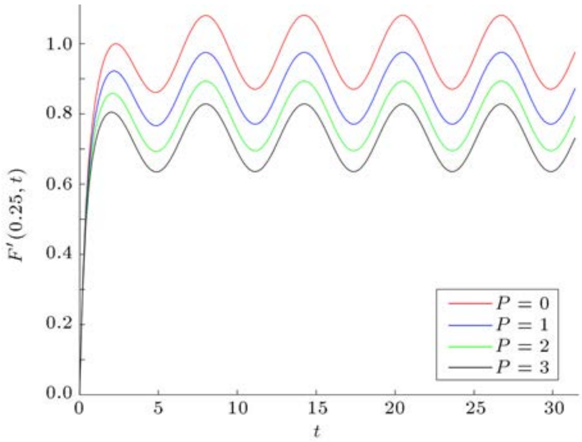

Figure 5. Out-turns of P on F' at $\eta = 0.25$.

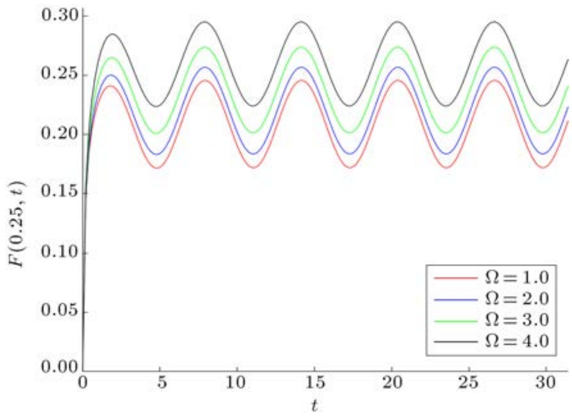

Figure 6. Out-turns of Ω on F at $\eta = 0.25$.

the tendency to decrease the velocity profiles. Here we pick $\eta = 0.25$. The dominance of swirl parameter on $F'(0.25, t)$ and $F(0.25, t)$ is prescribed in Figures 6 and 7, respectively. Here in case of swirl parameter, the domain of oscillatory profiles is slightly larger for both velocity curves in comparison to the oscillatory domain of porosity and magnetic parameters. The axial curves of velocity are close to each other as compared to the radial velocity profiles. As the swirl parameter and stretching rate keep inverse relation, then the amplifying values of Ω heighten the graphical

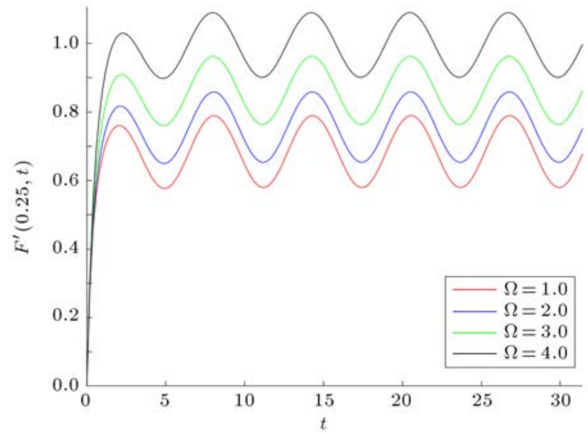

Figure 7. Out-turns of Ω on F' at $\eta = 0.25$.

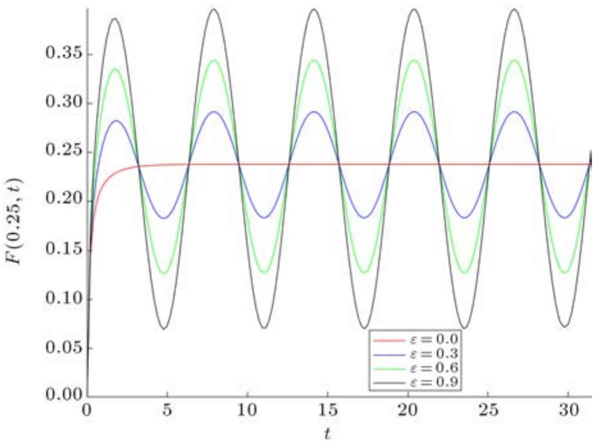

Figure 8. Out-turns of ε on F at $\eta = 0.25$.

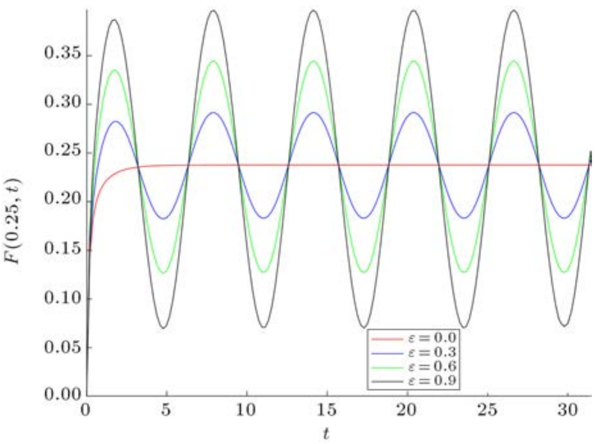

Figure 9. Out-turns of ε on F' at $\eta = 0.25$.

results. At initial level of time we observed small amplitudes related to oscillatory curves however with increasing time the amplitude increased due to fluid particles rapid thrust.

Various constant amplitude values on flow velocities are depicted in Figures 8 and 9. Both figures revealed the case of linearly rotating disk for $\varepsilon = 0$. In such case, the amplitude diminished. The non-

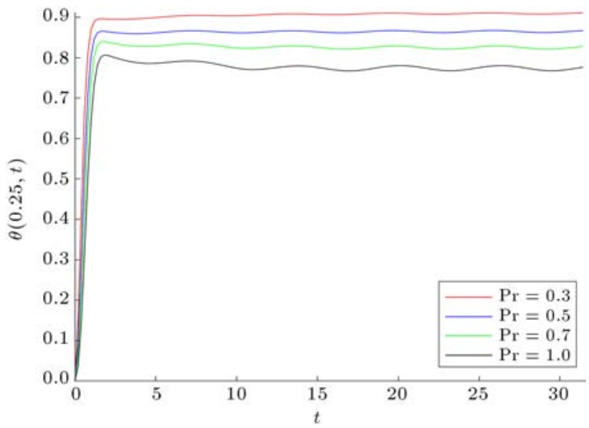

Figure 10. Out-turns of Pr on θ at $\eta = 0.25$.

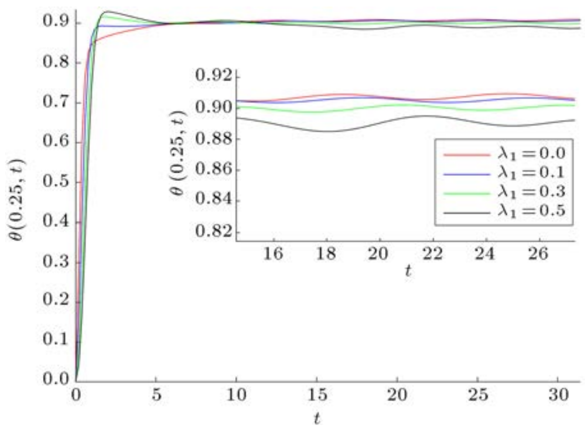

Figure 11. Out-turns of λ_1 on θ at $\eta = 0.25$.

zero declining miscellaneous values shrink the amplitude of oscillations. Moreover, amplitude interval for $F'(0.25, t)$ is larger than that of $F(0.25, t)$. Prandtl number illustration for distinct values of temperature filed is pictured in Figure 10. A rise in Prandtl number causes a reduction in temperature curves. For smaller values of Prandtl number the amplitudes of oscillatory temperature curves are very small however for larger Pr the amplitude of oscillations increases. A pictorial representation of thermal relaxation time parameter on $\theta(0.25, t)$ is shown in Figure 11. The increasing nature of λ_1 demands additional time for transformation of energy of molecules from one molecule to another; therefore profiles convey the decreasing behavior for increased λ_1. The oscillatory temperature curves are close to each other. Figure 11 also portrays the zooming figure in time interval $15 \leq t \leq 25$. Here phase difference is a notable feature in oscillatory temperature curve. The phase difference increases with an increase in λ_1. Similar observation is eminent for $\phi(0.25, t)$ from Figure 12 in scenario of enhancing λ_2. The consequences of various Schmidt number on $\phi(0.25, t)$ are illustrated in Figure 13. Schmidt number is responsible in decaying the oscillatory concentration curves. For smaller Schmidt number (Sc), the ampli-

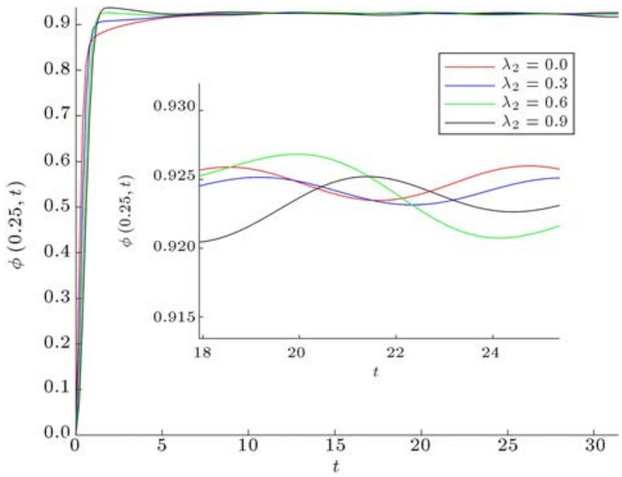

Figure 12. Out-turns of λ_2 on ϕ at $\eta = 0.25$.

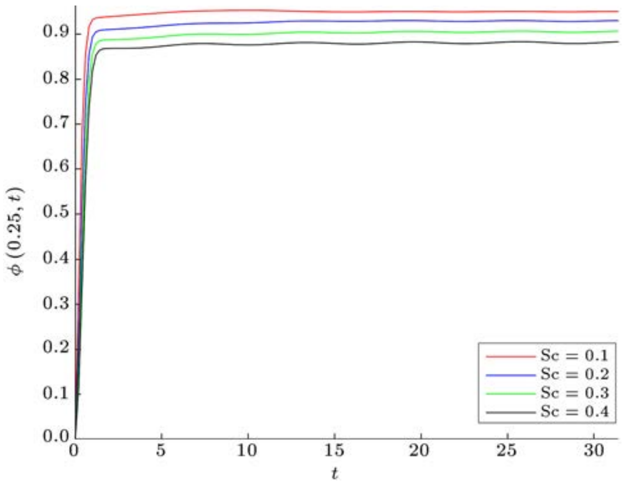

Figure 13. Out-turns of Sc on ϕ at $\eta = 0.25$.

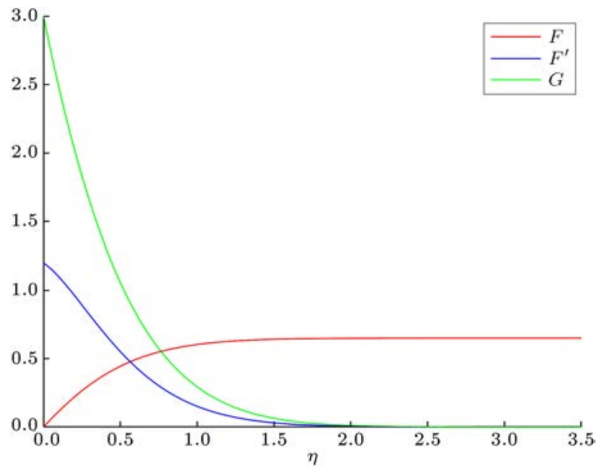

Figure 14. F, F' and G at $\eta = \pi/2$.

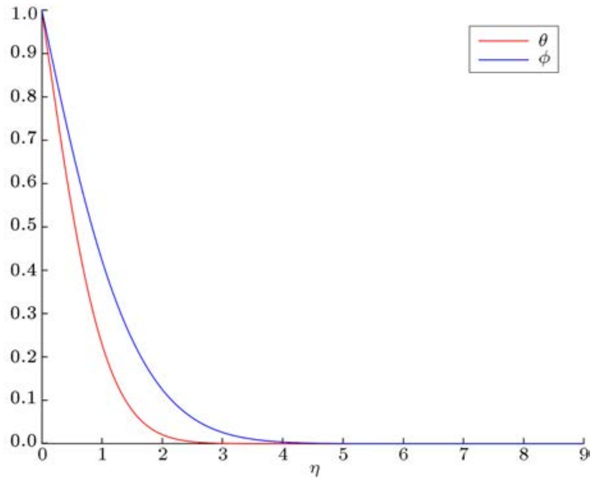

Figure 15. θ and ϕ at $\eta = \pi/2$.

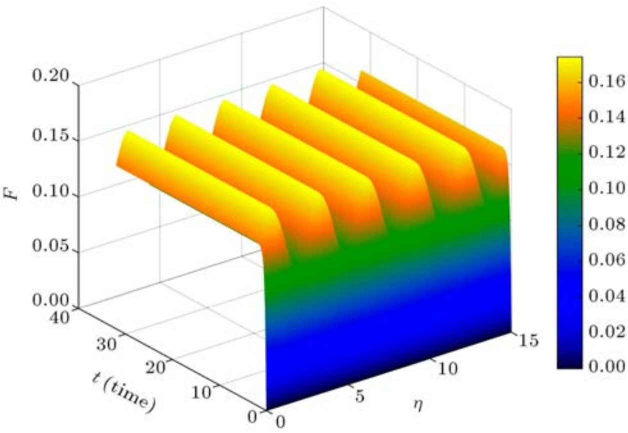

Figure 16. Flow behavior at η, t, and F.

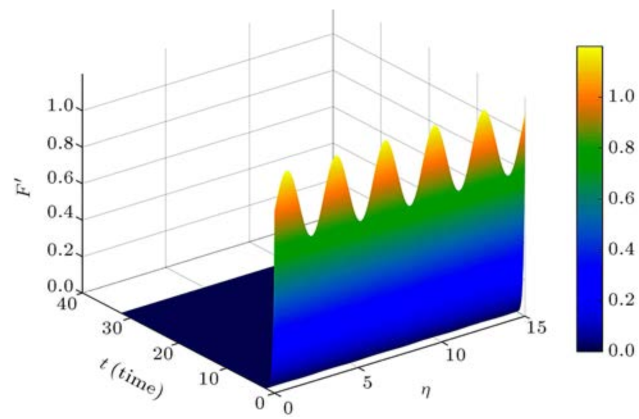

Figure 17. Flow behavior at η, t, and F'.

tude of oscillations is small while it tends to increase for larger Sc.

Figsures 14 and 15 are sketched for fixed values of $M = 0.5$, $P = 1$, $\varepsilon = 0.3$, $\Omega = 3$, $\Pr = 0.4$, $\mathrm{Sc} = \lambda_1 = \lambda_2 = 0.3$, $St = 0$ and $\eta = \pi/2$. The velocity curves are presented in Figure 14, while temperature and concentration curves are plotted in Figure 15. Both Figures 14 and 15 represent steady fluid flow phenomenon subject to linearly rotating disk. Three-dimensional demonstration of flow behavior is exhibited in Figures 16–20. Figures 16–18 depict the oscillatory flow phenomenon of axial, radial and tangential velocities, while Figure 19 and 20 reveal

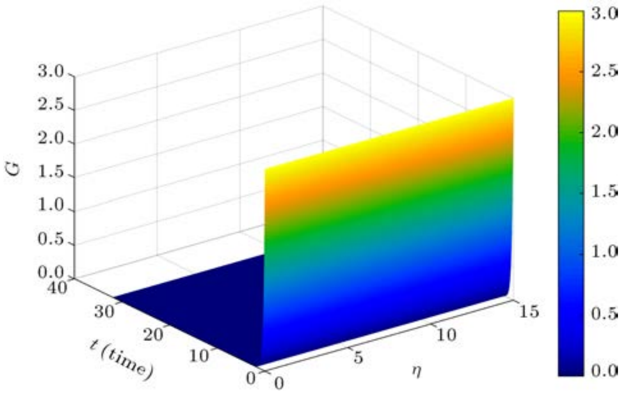

Figure 18. Flow behavior at η, t, and G.

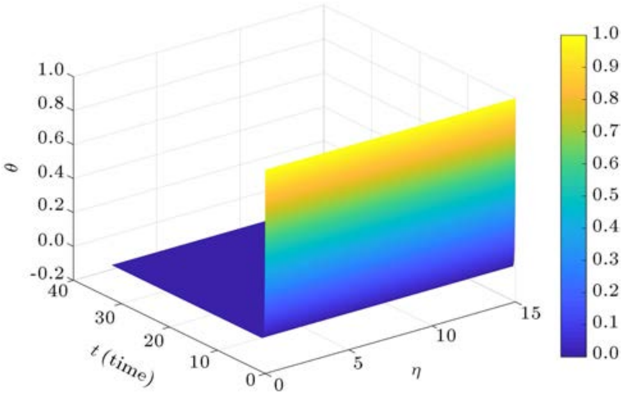

Figure 19. Flow behavior at η, t, and θ.

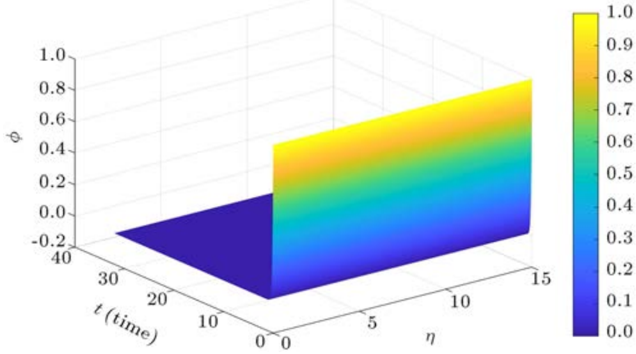

Figure 20. Flow behavior at η, t, and ϕ.

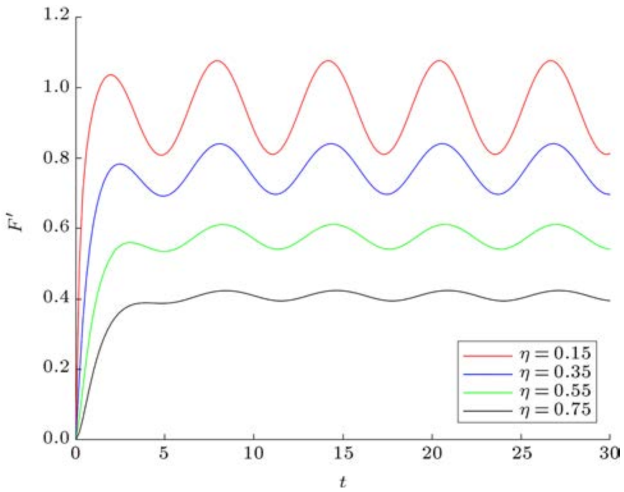

Figure 21. Various η on F' versus t.

flow behavior on temperature and concentration fields, respectively. Figure 21 describes the time series radial velocity curves considering numerous distances $\eta = 0.15, 0.35, 0.55, 0.75$ from disk surface. Because of the oscillatory disk, the curves amplitude is bigger nearby disk surface while away from disk the amplitudes tend to diminish.

Table 1 is constructed to examine the effect of magnetic and porosity parameters on frictional torque and radial shear stress. We consider several levels of time $t = \pi/6, \pi/4, \pi/2, 3\pi/4$. Magnetic parameter ranges from 0 to 2 and we considered the porosity parameter values from 0 to 3. The cases $M = 0$ and $P = 0$ represent hydrodynamic fluid flow which does not saturate the porous space. Increase in M and P enlarges frictional torque as well as radial shear stress for different time levels. The influence of Prandtl number and thermal relaxation time parameter on heat transfer rate is narrated in Table 2. The improved Pr and λ_1 grow up the rate of heat transfer for four different time scales. Table 3 illustrates the dominance of Schmidt number and concentration

Table 1. Numerical values of τ_{zr} and $\tau_{z\theta}$ for M and P considering four time levels.

M	P	$-\tau_{rz}$				$-\tau_{z\theta}$			
		$t=\pi/6$	$t=\pi/4$	$t=\pi/2$	$t=3\pi/4$	$t=\pi/6$	$t=\pi/4$	$t=\pi/2$	$t=3\pi/4$
0	1	0.1427	0.2365	0.3740	0.2163	5.0275	5.0691	5.1289	5.0602
1	1	0.6299	0.7278	0.8712	0.7067	5.7487	5.7862	5.8402	5.7782
1.5	1	1.1277	1.2318	1.3841	1.2094	6.5638	6.5986	6.6467	6.5915
2	1	1.6881	1.8016	1.9674	1.7721	7.5788	7.6068	7.6497	7.6016
0.5	0	0.0029	0.0977	0.0163	0.1175	4.4333	4.4780	4.5425	4.4684
0.5	1	0.2807	0.3753	0.5138	0.3549	5.2001	5.2404	5.2985	5.2318
0.5	2	0.7453	0.8441	0.9888	0.8228	5.9018	5.9381	5.9905	5.9303
0.5	3	1.1338	1.2376	1.3893	1.2152	6.5436	6.5767	6.6245	6.5696

Table 2. Numerical values of $-\theta'(0,t)$ for Pr and λ_1 considering four time levels.

Pr	λ_1	$-\theta'(0,t)$			
		$t=\pi/6$	$t=\pi/4$	$t=\pi/2$	$t=3\pi/4$
0.4	0.3	0.5319	0.5401	0.5520	0.5383
0.5	0.3	0.6383	0.6486	0.6635	0.6463
0.7	0.3	0.8318	0.8456	0.8658	0.8426
1	0.3	0.9526	1.0997	1.1266	1.0957
0.4	0	0.7770	0.7858	0.7985	0.7839
0.4	0.1	0.7924	0.8024	0.8167	0.8002
0.4	0.3	0.8429	0.8565	0.8763	0.8536
0.4	0.5	0.9230	0.9410	0.9674	0.9371

Table 3. Numerical values of $-\phi'(0,t)$ for Sc and λ_2 considering four time levels.

Sc	λ_2	$-\phi'(0,t)$			
		$t=\pi/6$	$t=\pi/4$	$t=\pi/2$	$t=3\pi/4$
0.3	0.3	0.4164	0.4226	0.4315	0.4212
0.4	0.3	0.5307	0.5390	0.5511	0.5372
0.5	0.3	0.6380	0.6482	0.6632	0.6460
0.7	0.3	0.8412	0.8523	0.8655	0.8424
0.3	0	0.4085	0.4128	0.4192	0.4119
0.3	0.3	0.4269	0.4326	0.4408	0.4314
0.3	0.6	0.4574	0.4652	0.4768	0.4636
0.3	0.9	0.5057	0.5169	0.5337	0.5145

relaxation time parameter on mass transfer rate under $t = \pi/6, \pi/4, \pi/2, 3\pi/4$. Expanding values of both parameters results in strengthening the mass transfer rate. In Table 4, the comparison of numerical values of shear and couple stresses by varying ε and Ω at distinct time levels is given. Excellent comparison endorses our numerically computed results.

5. Conclusions

The analysis is made through numerical technique for the problem of MHD viscous fluid flow through rotating disk. The fluid is caused due to disk oscillation. Cattaneo-Christov heat and mass flux models are implemented in energy and mass equation, respectively. The acquired system after using self-similar transformations is solved through SOR method. Key findings are pointed as:

1. The velocity graphs $F(0.25,t)$ and $F'(0.25,t)$ depict declining nature of increased magnetic and porosity parameters and increasing trend of enhanced swirl parameter such that the distance between profiles $F'(0.25,t)$ is larger as compared to $F(0.25,t)$;
2. The oscillatory amplitudes magnify for larger constant amplitude and when constant amplitude is zero, the amplitude diminishes;
3. Thermal and concentration relaxation time parameters have reducing trend in temperature and concentration fields, respectively. Furthermore phase-log in oscillatory curves is also noticed in such profiles;
4. Time concentration profiles are reduced for larger Schmidt number, and smaller oscillations are observed in profiles;
5. Intensifying values of thermal relaxation time parameter and Prandtl number strengthens heat transfer rate against $t = \pi/6, \pi/4, \pi/2, 3\pi/4$;
6. Mass transfer rate is enlarged for enhanced concentration relaxation time parameter and Schmidt number considering various time levels.

Acknowledgements

The authors are grateful to the reviewers for their useful comments and suggestions to improve the quality of the manuscript. They extend their appreciation to the Deanship of Scientific Research at King Khalid University for funding this work through Research Groups Program under grant number (R.G.P2./66/40).

Table 4. Comparison of τ_{zr} and $\tau_{z\theta}$ for ε and Ω considering distinct time levels.

ε	Ω	$-\tau_{zr}$				$-\tau_{z\theta}$			
		$t=\frac{\pi}{6}$ [37]	$t=\frac{\pi}{6}$ [Present]	$t=\frac{\pi}{4}$ [37]	$t=\frac{\pi}{4}$ [Present]	$t=\frac{\pi}{6}$ [37]	$t=\frac{\pi}{6}$ [Present]	$t=\frac{\pi}{4}$ [37]	$t=\frac{\pi}{4}$ [Present]
0.3	3	0.4010	0.4010	0.5450	0.5450	5.2681	5.2681	5.3283	5.3283
0.6	3	0.7915	0.7915	1.0902	1.0902	5.4285	5.4285	5.5457	5.5457
0.9	3	1.1941	1.1941	1.6581	1.6581	5.5854	5.5854	5.7567	5.7567
0.3	1	1.6300	1.6300	1.7113	1.7113	1.6533	1.6533	1.6686	1.6686
0.3	2	1.1029	1.1029	1.1913	1.1913	3.3762	3.3762	3.4051	3.4051
0.3	3	0.2736	0.2736	0.3684	0.3684	5.2139	5.2139	5.2543	5.2543

Nomenclature

γ	Angular speed of disk
(u, ν, w)	Velocity components
C_w	Wall concentration
C_∞	Ambient concentration
ρ	Density
β_0	Magnetic flux density
ϕ_1	Porosity of porous medium
$\alpha = \dfrac{k}{\rho c_p}$	Coefficient of heat diffusion
τ_0	Heat flux relaxation time
τ_1	Concentration relaxation time
t	Time
$St = \dfrac{\omega}{a}$	Unsteady parameter
$P = \dfrac{\mu\phi_1}{a\rho k_1}$	Porosity parameter
$\Omega = \dfrac{\gamma}{a}$	Swirl parameter
$\lambda_2 = a\tau_1$	Concentration relaxation time parameter
$\mathrm{Re}_x = \dfrac{ar^2}{\upsilon}$	Local Reynolds number
ε	Amplitude
T_w	Wall temperature
T_∞	Ambient temperature
υ	Kinematic viscosity
μ	Viscosity
σ_e	Electrical conductivity
k_1	Permeability of porous medium
D_B	Brownian diffusion
ω	Angular frequency
$(')$	Differentiation with respect to dimensionless variable z
a	Stretching strength
$M = \sqrt{\dfrac{\sigma_e\beta_0^2}{a\rho}}$	Magnetic parameter
$\mathrm{Pr} = \dfrac{\upsilon}{\alpha}$	Prandtl number
$\lambda_1 = a\tau_0$	Thermal relaxation time parameter
$\mathrm{Sc} = \dfrac{\upsilon}{D_B}$	Schmidt number
$\rho(G_{\mathrm{Jac}})$	Spectral radius of Jacobi method

References

1. Bargmann, S. and Steinmann, P. "On the propagation of second sound in linear and non-linear media, results from Green-Naghdi theory", *Phys. Lett. A*, **372**, pp. 4418–4424 (2008).
2. Christov, C.I. "On frame indifferent formulation of the Maxwell-Cattaneo model of finite-speed heat conduction", *Mech. Research Commun.*, **36**, pp. 481–486 (2009).
3. Khan, W.A., Khan, M., and Alshomrani, A.S. "Impact of chemical processes on 3D Burgers fluid utilizing Cattaneo-Christov double-diffusion: Applications of non-Fourier's heat and non-Fick's mass flux models", *J. Mol. Liq.*, **223**, pp. 1039–1047 (2016).
4. Liu, L., Zheng, L., Liu, F., and Zhang, X. "An improved heat conduction model with Riesz fractional Cattaneo-Christov flux", *Int. J. Heat Mass Transf.*, **103**, pp. 1191–1197 (2016).
5. Upadhay, M.S., Mahesha, and Raju, C.S.K. "Cattaneo-Christov on heat and mass transfer of unsteady Eyring Powell dusty nanofluid over sheet with heat and mass flux conditions", *Inform. Med. Unlock.*, **9**, pp. 76–85 (2017).
6. Farooq, M., Ahmad, S., Javed, M., and Anjum, A. "Analysis of Cattaneo-Christov heat and mass fluxes in the squeezed flow embedded in porous medium with variable mass diffusivity", *Results Phys.*, **7**, pp. 3788–3796 (2017).
7. Shehzad, S.A., Hayat, T., Alsaedi, A., and Meraj, M.A. "Cattaneo-Christov heat and mass flux model for 3D hydromagnetic flow of chemically reactive Maxwell liquid", *Appl. Math. Mech.*, **38**, pp. 1347–1356 (2018).
8. Rauf, A., Abbas, Z., Shehzad, S.A., Alsaedi, A., and Hayat, T. "Numerical simulation of chemically reactive Powell-Eyring liquid flow with double diffusive Cattaneo-Christov heat and mass flux theories", *Appl. Math. Mech.*, **39**, pp. 467–476 (2018).
9. Aqsa, Malik, M.Y., Imtiaz, A., and Awais, M. "Rheology of Burgers' model with Cattaneo-Christov heat flux in the presence of heat source/sink and magnetic field", *Sci. Iran.*, **26**, pp. 323–330 (2019).
10. Khan, S.U., Shehzad, S.A., Ali, N., and Bashir, M.N. "Analysis of second-grade fluid flow in porous channel with Cattaneo-Christov and generalized Fick's theories", *Sci. Iran.*, **27**, pp. 1945–1954 (2020).
11. Chawla, S.S., Srivastava, P.K., and Gupta, A.S. "Rotationally symmetric flow over a rotating disk", *International Journal of Non-Linear Mechanics*, **44**, pp. 717–726 (2009).
12. Mahmood, K., Sajid, M., Ali, N., and Javed, T. "Heat transfer analysis in the time-dependent slip flow over a lubricated rotating disc", *Eng. Sci. Tech., an Int. J.*, **19**, pp. 1949–1957 (2016).
13. Yin, C., Zheng, L., Zhang, C., and Zhang, X. "Flow and heat transfer of nanofluids over a rotating disk with uniform stretching rate in the radial direction", *Prop. Power Research*, **6**, pp. 25–30 (2017).
14. Mustafa, M. "MHD nanofluid flow over a rotating disk with partial slip effects: Buongiorno model", *Int. J. Heat Mass Transf.*, **108**, pp. 1910–1916 (2017).
15. Turkyilmazoglu, M. "Fluid flow and heat transfer over a rotating and vertically moving disk", *Phys. Fluids*, **30**, p. 063605 (2018).

16. Lok, Y.Y., Merkin, J.H., and Pop, I. "Axisymmetric rotational stagnation-point flow impinging on a permeable stretching/shrinking rotating disk", *Euro. J. Mech.-B/Fluids*, **72**, pp. 275–292 (2018).
17. Hayat, T., Khan, M.I., Qayyum, S., Khan, M.I., and Alsaedi, A. "Entropy generation for flow of Sisko fluid due to rotating disk", *J. Mol. Liq.*, **264**, pp. 375–385 (2018).
18. Gholinia, M., Hosseinzadeh, K., Mehrzadi, H., Ganji, D.D., and Ranjbar, A.A. "Investigation of MHD Eyring-Powell fluid flow over a rotating disk under effect of homogeneous-heterogeneous reactions", *Case Stud. Therm. Eng.*, **13**, p. 100356 (2018).
19. Liu, Q. and He, Y. "Lattice Boltzmann simulations of convection heat transfer in porous media", *Phys. A: Stat. Mech. Appl.*, **465**, pp. 742–753 (2017).
20. Jourabian, M., Darzi, A.A.R., Toghraie, D., and Akbari, O.A. "Melting process in porous media around two hot cylinders: Numerical study using the lattice Boltzmann method", *Phys. A: Stat. Mech. Appl.*, **509**, pp. 316–335 (2018).
21. Kefayati, G.H.R. "Lattice Boltzmann method for natural convection of a Bingham fluid in a porous cavity", *Phys. A: Stat. Mech. Appl.*, **521**, pp. 146–172 (2019).
22. Jahanbakshi, S., Pishvaie, M.R., and Boozarjomehry, R.B. "Characterization of three-phase flow in porous media using the ensemble Kalman filter", *Sci. Iran.*, **24**, pp. 1281–1301 (2017).
23. Ghaffarpasand, O. and Fazeli, D. "Numerical analysis of MHD mixed convection flow in a parallelogramic porous enclosure filled with nano fluid and in presence of magnetic field induction", *Sci. Iran.*, **25**, pp. 1789–1807 (2018).
24. Nuori-Borujerdi, A. "A new approach to thermo-Fluid behavior through porous layer of heat pipes", *Sci. Iran.*, **25**, pp. 1236–1242 (2018).
25. Sheikholeslami, M., Ganji, D.D., Li, Z., and Hosseinnejad, R. "Numerical simulation of thermal radiative heat transfer effects on Fe_3O_4-Ethylene glycol nanofluid EHD flow in a porous enclosure", *Sci. Iran.*, **26**(3), pp. 1405–1414 (2018). doi:10.24200/SCI.2018.5567.1348.
26. Darcy, H.R.P.G., *Les Fontaines Publiques de la Volle de Dijon*, Vector Dalmont. Paris (1856).
27. Attia, H.A. "Asymptotic solution for rotating disk flow in porous medium", *Mech. Mech. Eng.*, **14**, pp. 119–136 (2010).
28. Khan, S.U., Ali, N., and Abbas, Z. "Hydromagnetic flow and heat transfer over a porous oscillating stretching surface in a viscoelastic fluid with porous medium", *Plos One*, **10**, p. 0144299 (2015).
29. Ali, N., Khan, S.U., Sajid, M., and Abbas, Z. "MHD flow and heat transfer of couple stress fluid over an oscillatory stretching sheet with heat source/sink in porous medium", *Alex. Eng. J.*, **55**, pp. 915–924 (2016).
30. Ali, N., Khan, S.U., Sajid, M., and Abbas, Z. "Slip effects in the hydromagnetic flow of a viscoelastic fluid through porous medium over a porous oscillatory stretching sheet", *J. Porous Med.*, **20**, pp. 249–262 (2017).
31. Hasnain, J. and Abbas, Z. "Hydromagnetic convection flow in two immiscible fluids through a porous medium in an inclined annulus", *J. Porous Med.*, **20**, pp. 977–987 (2017).
32. Sheikholeslami, M. and Shehzad, S.A. "CVFEM simulation for nanofluid migration in a porous medium using Darcy model", *Int. J. Heat Mass Transf.*, **122**, pp. 1264–1271 (2018).
33. Sheikholeslami, M., Kataria, H.R., and Mittal, A.S. "Effect of thermal diffusion and heat-generation on MHD nanofluid flow past an oscillating vertical plate through porous medium", *J. Mol. Liq.*, **257**, pp. 12–25 (2018).
34. Rauf, A., Abbas, Z., and Shehzad, S.A. "Utilization of Maxwell-Cattaneo law for MHD swirling flow through oscillatory disk subject to porous medium", *Appl. Math. Mech.*, **40**, pp. 837–850 (2019).
35. Munawar, S., Ali, A., Saleem, N., and Naqeeb, A. "Swirling flow over an oscillatory stretchable disk", *J. Mech.*, **30**, pp. 339–347 (2014).
36. Rauf, A., Abbas, Z., and Shehzad, S.A. "Chemically hydromagnetic flow over a stretchable oscillatory rotating disk with thermal radiation and heat source/sink: A numerical study", *Heat Transf. Research*, **50**, pp. 1495–1512 (2019).
37. Rauf, A., Abbas, Z., and Shehzad, S.A. "Interactions of active and passive control of nanoparticles on radiative magnetohydrodynamics flow of nanofluid over oscillatory rotating disk in porous medium", *J. Nanofluids*, **8**, pp. 1385–1396 (2019).
38. Milne, W.E., *Numerical Solutions of Differential Equations*, John Willey and Sons Inc., New York (1953).
39. Hachbusch, W., *Iterative Solution of Large Sparse Systems of Equations*, Springer International Publishing, Switzerland (2016).

Biographies

Zaheer Abbas is an Associate Professor in the Department of Mathematics, the Islamia University of Bahawalpur, Bahawalpur, Pakistan. He earned his PhD in Applied Mathematics from Quaid-I-Azam University, Islamabad in 2010. His research interests include Newtonian and non-Newtonian fluids flow, fluid flow in porous medium, heat and mass transfer, magnetohydrodynamics, and fluid dynamics of peristaltic flows.

Amar Rauf is PhD scholar at Department of Mathematics, the Islamia University Bahawalpur, Pakistan. He is also working as a Lecturer at COMSATS University Islamabad, Sahiwal Campus since 2014. He is working on Newtonian and non-Newtonian nanofluids under various flow geometries and different physical aspects. He has published more than 30 research articles in different journals of high repute.

Sabir Ali Shehzad is working as an Assistant Professor at Department of Mathematics, COMSATS University Islamabad, Sahiwal Pakistan. He has received his PhD in Fluid Mechanics from Quaid-I-Azam University, Islamabad, Pakistan in 2014. His main research interests are Newtonian and non-Newtonian fluids, nanofluids and heat and mass transfer analysis. He has published more than 300 research articles in various high reputed international journals.

Metib Alghamdi is an Assistant Professor in Applied Mathematics in the Department of Mathematics, King Khalid University Abha, Saudi Arabia. His main interest covers applied mathematics, Newtonian and non-Newtonian fluid flows and heat transfer analysis.